Nuclear Theory'25
ed. S. Dimitrova, Heron Press, Sofia, 2006

# g-factor measurement at RISING: The case of $^{127}$Sn

**L. Atanasova**[1], **D. L. Balabanski**[2,3], **M. Hass**[4], **D. Bazzacco**[5], **F. Becker**[6], **P. Bednarczyk**[6,7], **G. Benzoni**[8], **N. Blasi**[8], **A. Blazhev**[9], **A. Bracco**[8], **C. Brandau**[6,10], **L. Caceres**[6,11], **F. Camera**[8], **S. K. Chamoli**[4], **F. Crespi**[8], **P. Detistov**[1], **P. Doornenbal**[6], **C. Fahlander**[12], **E. Farnea**[5], **G. Georgiev**[13], **J. Gerl**[6], **K. Gladnishki**[3], **M. Górska**[6], **H. Grawe**[6], **J. Grebosz**[6,7], **R. Hoischen**[12], **G. Ilie**[9], **M. Ionescu-Bujor**[14], **A. Iordachescu**[14], **A. Jungclaus**[11], **G. Lo Bianco**[3], **M. Kmiecik**[7], **I. Kojouharov**[6], **N. Kurz**[6], **S. Lakshmi**[4], **R. Lozeva**[1,15], **A. Maj**[7], **D. Montanari**[8], **G. Neyens**[15], **M. Pfützner**[16], **S. Pietri**[10], **Zs. Podolyák**[10], **W. Prokopowicz**[6,7], **D. Rudolph**[12], **G. Rusev**[17], **T. R. Saito**[6], **A. Saltarelli**[3], **H. Schaffner**[6], **R. Schwengner**[17], **G. Simpson**[18], **S. Tachenov**[6], **J. J. Valente-Dubon**[19], **N. Vermeulen**[15], **J. Walker**[6,10], **E. Werner-Malento**[6,16], **O. Wieland**[8], **H. J. Wollersheim**[6]

[1]Faculty of Physics, University of Sofia, BG-1164 Sofia, Bulgaria
[2]INRNE, Bulgarian Academy of Sciences, BG-1784 Sofia, Bulgaria
[3]Universitá di Camerino and INFN-Perugia, 62032 Camerino, Italy
[4]Weizmann Institute of Science, Rehovot 76100, Israel
[5]Universitá di Padova and INFN-Padova, 35131 Padova, Italy
[6]GSI, Planckstrasse 1, D-64291, Darmstadt, Germany
[7]INP, Polish Academy of Sciences, PL-31 342 Krakow, Poland
[8]Universitá di Milano and INFN-Milano, 20133 Milano, Italy
[9]IKP, Universität zu Köln, D-50937, Köln, Germany
[10]Department of Physics, University of Surrey, Guildford, GU2 7XH, UK
[11]Departamento de Fisica Teórica, Universidad Autonoma de Madrid, Spain
[12]Department of Physics, Lund University, S-22100 Lund, Sweden
[13]CSNSM, F-91405 Orsay Campus, France
[14]NIPNE, P.O. Box MG-6, Bucharest, Romania
[15]IKS, K.U.Leuven, Celestijnenlaan 200D, 3001 Leuven, Belgium
[16]IEP, Warsaw University, PL-00-681 Warsaw, Poland
[17]Forschungszentrum Rossendorf, D-01314, Dresden, Germany
[18]LPSC, 38026 Grenoble Cedex, France
[19]INFN - Laboratori Nazionali di Legnaro, 35020 Legnaro (Padova), Italy

**Abstract.**

We report results of a $g$-factor measurement of the $19/2^+$ $T_{1/2} = 4.5(3)$ $\mu$s isomer in $^{127}$Sn, which were carried out within the g-RISING project at GSI, Darmstadt, Germany. The time-differential perturbed angular distribution (TDPAD) method was utilized in the experiment. Isomers in $A \approx 130$ nuclei were populated in relativistic projectile fragmentation of a $^{136}$Xe beam at $E/A = 600$ MeV/u on a 1024 mg/cm$^2$ Be production target. Fully-stripped ions were separated with the fragment separator (FRS), which allowed the preservation of the orientation of the nuclear spin ensemble as obtained in the reaction. The ions were implanted in a Copper plate, which provided a perturbation-free environment for the isomeric $\gamma$ decay. The nuclei of interest were tracked and identified on an event-by-event basis and ion-$\gamma$ coincidences were recorded. The $\gamma$ rays deexciting the isomers were detected with eight Cluster Ge detectors mounted in the horizontal plane perpendicular to a 0.12 T external magnetic field.

## 1 Introduction

The g-RISING experimental campaign was carried out at the GSI laboratory in Darmstadt, Germany within a RISING (Rare ISotope INvestigations at GSI) project [1] and aimed at studies $g$ factors of isomers in exotic nuclei far from stability which were populated in beam fragmentation or projectile fission at relativistic energies. Isomers have a rather pure single particle configuration in regions of doubly-magic nuclei. Measurements of their $g$ factors can provide information about their wave functions and their purity. They can confirm suggested spin and party assignments, especially in regions far from stability, where they are based on theoretical predictions or analogy with neighbouring nuclei.

Three experiments were approved for the g-RISING campaign. Two of them aimed at studies of isomeric $g$ factors in the vicinity of the doubly-magic $^{132}$Sn. The isomers of interest were populated in the fragmentation of $^{136}$Xe beam in the first case, and in relativistic fission of the $^{238}$U in the second. This makes possible the direct comparison of the spin-alignment in fragmentation and fission reactions at relativistic energies and provides two independent measurements of the $g$ factor of the $19/2^+$, $T_{1/2} = 4.5(3)$ $\mu$s isomer in $^{127}$Sn [2]. Here we report the status of the analysis of the fragmentation experiment.

The configurations of the isomeric states in Sn isotopes below $N = 82$ shell gap consist of neutron holes in $d_{3/2}$, $h_{11/2}$ and $s_{1/2}$ shell model orbits. The corresponding empirical $g$ factors of these states, which based on experimental measurements of single-particle configurations, are $g_{emp}(d_{3/2}) \approx 0.50$, $g_{emp}(h_{11/2}) \approx -0.24$ and $g_{emp}(s_{1/2}) \approx -2.1$. For non-pure shell model states, the $g$ factor depends also on the configuration mixing.

Microsecond $19/2^+$ isomers were observed in the odd-$A$ Sn isotopes with masses between $A = 119$ and $A = 129$ [3]. The spin and parity assignments

for the isomer in $^{127}$Sn are based on energy systematic and comparison with theoretical calculations. The excitation energies of the $19/2^+$ states are similar to these of the $5^-$ isomers in the neighbouring even-even Sn isotopes. Thus, it was suggested [2] that the main component of the wave function of the isomeric level is $(\nu h_{11/2}^{-1} \otimes 5^-)_{19/2+}$. The measured g-factor of the $5^-$ isomers is $g \approx -0.067(13)$ [4] which suggests that the major contribution in the $5^-$ wave function is due to the $(\nu s_{1/2}^{-1} h_{11/2}^{-1})$ configuration, which has an empirical $g$ factor of $g_{emp} \approx -0.093$.

The $19/2^+$ isomers was suggested to decay partially via strongly hindered transitions of predominantly M2 character to $15/2^-$ states in $^{123-127}Sn$ (see the right-hand-side of Figure 5 for the case of $^{127}$Sn). This state, together with the $11/2^-$ and $13/2^-$ states are expected to be rather pure members of the $h_{11/2}$ multiplet. Because of the change of parity, this transition cannot take place between states with the $(\nu h_{11/2}^{-3})$ and $(\nu s_{1/2}^{-1} h_{11/2}^{-2})$ configurations and an admixture of $(\nu g_{7/2}^{-1} h_{11/2}^{-2})$ is suggested in the wave function [2]. Both configurations have different g-factors: $g_{emp}(s_{1/2}^{-1} h_{11/2}^{-2}) \approx -0.156$ and $g_{emp}(g_{7/2}^{-1} h_{11/2}^{-2}) \approx -0.23$, so the experiment will determine whether the suggested configuration is correct and what is the amount of admixture.

For the measurement of $g$ factors of interest we applied the Time Dependent Perturbed Angular Distribution (TDPAD) method, which is based on measuring the perturbation of the $\gamma$-anisotropy of the spin-oriented nuclear ensemble due to externally applied magnetic field. Prior this experiment several TDPAD measurements on isomers produced in fragmentation reactions at relativistic [5] and intermediate energies [6, 7] of the primary beam were performed. A major requirement to study of nuclear electromagnetic moments is to observe the decay of a spin-oriented ensemble. In fragmentation reactions, spin orientation of the isomers is obtained in the reaction itself and it is necessary to preserve the produced alignment to the implantation point. As the isomers are in-flight mass separated, the hyperfine interaction between the nuclear and random oriented electron spin can destroy the orientation of the nuclear ensemble. The fragments are produced fully stripped due to the high energy of the primary beam. The pick-up of electrons increases with $Z$ of the ions for similar beam energy and decreases with the beam energy for ions with the same $Z$. This limits the opportunities to perform such experiments at intermediate energies of the primary beam ($60 - 100$ MeV/u) to masses $A \leq 80$. For heavier nuclei such experiments can be done only with relativistic beams, which are available at GSI.

## 2 Experiment

The neutron-rich nuclei around $A \approx 130$ were produced in relativistic projectile fragmentation of a $^{136}$Xe beam at $E/A = 600$ MeV/u on a thin 1024 mg/cm$^2$ Be production target. The primary beam, which had an average intensity of $2 \cdot 10^9$ ions per a 10 s spill, was provided by the GSI heavy ion synchrotron

(SIS). The fully-stripped ions were separated and identified with the two-stage high resolution magnetic zero-degree FRagment Separator (FRS) [8], which was operated in the standard achromatic mode. A schematic view of the set-up is shown in Figure 1.

The longitudinal momentum distribution of the fragments was measured by scintillator detector *Sc21* in the second focal plane of FRS ($S2$). In front of it slits were introduced to cut the primary beam. The time of flight, measured with scintillator detectors *Sc21* and *Sc41* (see Figure 1) together with the magnetic rigidity of the beam $B\rho$ was used to determine the mass-to-charge ratio, $A/q$. The ion charge $Z$ was determined by the energy loss in the MUlti-Sampling Ionization Chamber (MUSIC) at the final focus. This allows the identification of the ions which reach the final focus of the FRS, as shown in Figure 2. The multiwire proportional chambers, *Mw41* and *Mw42*, together with the position

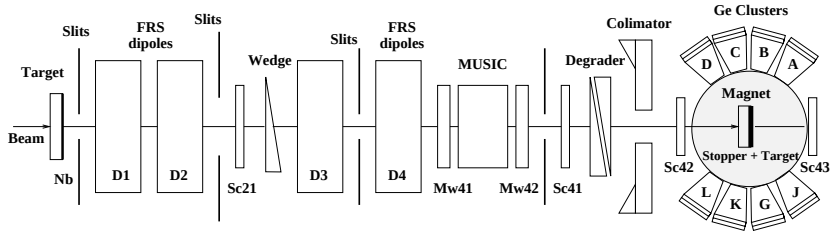


Figure 1. Schematic view of the experimental set-up, consisting of the FRS, the beam-line detectors, the $\gamma$-ray detectors and an electromagnet (see for explanations in the text).

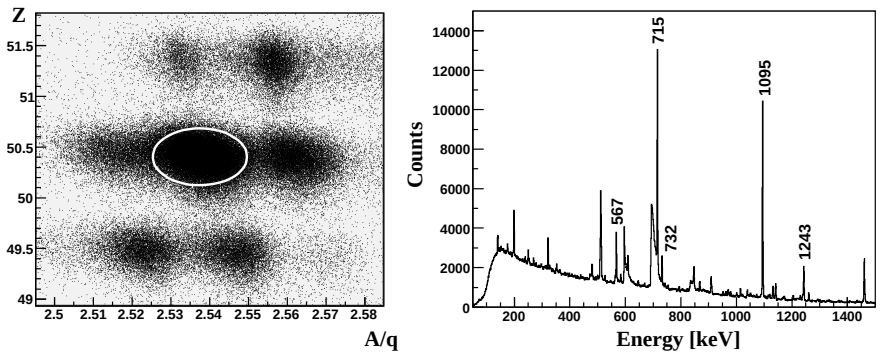


Figure 2. Left: Typical identification plot; the ellipse indicates the gate on $^{127}$Sn. The spots left and right of it correspond to $^{126}$Sn and $^{128}$Sn, respectively, while these up are for $^{129}$Sb and $^{130}$Sb, and down for $^{124}$In and $^{125}$In. Right: Energy spectrum for $^{127}$Sn gated on the identification plot. The labelled transitions belong to the decay of the $19/2^+$ isomer.

information from *Sc21*, were used for the precise beam tracking of each ion.

The $^{127}$Sn secondary beam was transported through the FRS with an energy of 300 MeV/u. At the final focal plane of FRS ($S4$) the ions were stopped by using a thick 15 mm Plexiglas degrader which was glued in front of a high-purity (99.998%) 2 mm annealed Copper plate which served as an implantation host. It has a cubic lattice, without electric field gradients, and provided a perturbation-free environment for the implanted ions. It was placed between the poles in the center of an electromagnet that provided a constant magnetic field $\vec{B}$ in the vertical direction. The magnet was shielded upstream with a Pb brick wall. The beam entered the magnet through a hole in the yoke with a diameter of 70 mm. Upstream a Pb collimator was built in in the Pb wall with a diameter of 50 mm. In this way, the beam spot at the secondary target position had a diameter of 50 mm. Two additional scintillator detectors, *Sc42* and *Sc43*, were placed in front and behind the catcher, which allows to validate the implantation of the impinging ions.

The isomeric $\gamma$ rays were detected with eight Cluster Ge detectors mounted in the horizontal plane perpendicular to the magnetic field. A Cluster detector consists of seven tapered hexagonal Ge crystals in a common cryostat. Each crystal can act as a separate detector. The average distance from the stopper to the front face of the detectors was approximately 43 cm. The total $\gamma$-ray efficiency was measured by placing a calibrated $^{152}$Eu source placed at six different positions at the catcher, covering the whole implantation spot and is approximately $2\%$ at 1000 keV. In Figure 2 (right) is presented an isotope gated energy spectrum. The $19/2^+$ isomer decay lines of $^{127}$Sn are labeled. There are some contaminating transitions from neighbouring Sn isotopes and background lines in the spectrum.

The nuclei of interest were identified on an event-by-event basis. Coincidences between ion signals from the FRS detectors and $\gamma$ rays detected with the Ge detectors were recorded within a time window of 12 $\mu$s, provided by a common time-to-amplitude converter. In addition, signals from the each crystal of the Cluster detectors were sent to an individual TDC, which opened an additional 2 $\mu$s window. This allows successive isomers to be studied, as well as to time-align the individual crystals. The fast signal from *Sc41* which was generated by an impinging ion was used to start the time measurement ($t = 0$ signal). The measured time spectrum for the $19/2^+$ isomer in $^{127}$Sn is presented in the top section of Figure 3.

The magnetic field $B = 0.12$ T was chosen such that with the minimal expected $g$ factor of $g = -0.1$ to have at least two periods in the $R(t)$ function, as demonstrated in the bottom part of Figure 3. The direction of the magnetic field was switched manually at every four hours during the experiment.

## 3 Data Analysis

Within the present experiment in total $2 \cdot 10^5$ single-hit photopeak events ( $2.5 \cdot 10^5$ photopeak events in add-back mode), which belong to the $\gamma$-decay of the $19/2^+$ isomer in $^{127}$Sn, were detected. In order to extract the experimental $R(t)$ function, it is necessary to apply conditions on the longitudinal momentum distribution, by selecting events which belong either to the center, or to the wing. This reduces the numbers of events which are used in the data analysis, as presented in Table 1. At this stage of the analysis only single-hits in each Cluster were considered.

Table 1. Statistics for the measured $\gamma$ rays belonging to the decay of the $19/2^+$ isomer in $^{127}$Sn for all detectors, and for both directions of the magnetic field.

| | 1095 keV | 732 keV | 715 keV |
|---|---|---|---|
| Center | 23980 | 8360 | 33590 |
| Wing | 13700 | 4870 | 19030 |
| Total | 68100 | 23700 | 94900 |
| Total after background subtraction | 66435 | 6318 | 58998 |

### 3.1 The $R(t)$ functions

The constant magnetic field $B$ induces rotation of the spins of the aligned nuclear ensemble around the magnetic field axis with a Larmour frequency

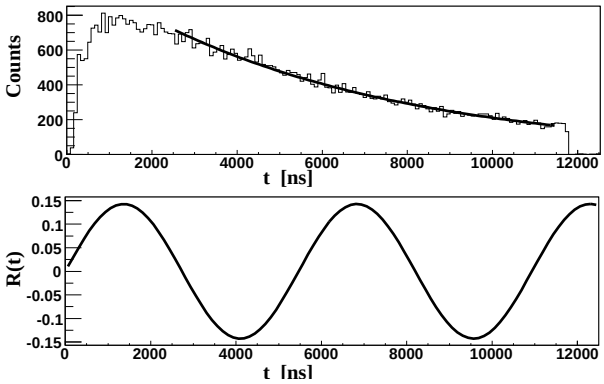


Figure 3. Top: Time spectrum for the 1095 keV line in $^{127}$Sn with the half-life of 4.5(3) $\mu$s; Bottom: Calculated R(t) function assuming $g = -0.1$ and a magnetic field $B = 0.12$ T

$\omega_L = -g\mu_N B/\hbar$ which depends of the isomeric g-factor and applied magnetic field. The intensity of the $\gamma$ decay, detected in the horizontal plane at an angle $\theta$ with respect to the beam axis is related to the angular distribution:

$$I(t,\theta,B) = I_0 e^{-\lambda t} W(t,\theta,B) \\ = I_0 e^{-\lambda t}\{1 + A_2(\gamma)B_2 P_2[(cos(\theta - \omega_L t - \alpha))]\}. \quad (1)$$

Here $A_2(\gamma)$ is the angular distribution coefficient, depending on the details of the $\gamma$ decay, $B_2$ is the orientation parameter, depending of the degree of alignment produced in the reaction. $P_2(cos(\theta))$ is the $2^{nd}$ order Legendre Polynomial and $\alpha$ is the angle between the beam direction and the symmetry axis of the spin-oriented ensemble, which in this case is equal to zero, because FRS is a zero-degree fragment separator. We neglect the $4^{th}$ and higher order components, because they are usually about an order of magnitude smaller.

To extract the precession pattern from measured time spectra, they are combined in $R(t)$ functions for each $\gamma$ transition

$$R(t,\theta,\theta',B) = \frac{I_1(t,\theta,B) - I_2(t,\theta',B)}{I_1(t,\theta,B) + I_2(t,\theta',B)}, \quad (2)$$

where $I_1$ stays for the time spectrum of a detector placed at an angle $\theta$ with respect to the beam, and $I_2$ is the time spectrum for a detector at an angle $\theta'$. This expression does not dependent on the isomeric decay constant. It has highest amplitude for the detectors placed at $90^\circ$ with respect to each other and at $\pm 45^\circ$ and $\pm 135^\circ$ with respect to beam axis, provided that $\alpha = 0$.

$$R(t,B) = \frac{3A_2B_2}{4 + A_2B_2}\sin(2\omega t). \quad (3)$$

It is possible to compose an $R(t)$ using the data from the same detector but for two opposite directions of the magnetic field. For detector placed at angle $\theta$ we obtain

$$R(t,\theta,\pm B) = \frac{3A_2B_2 sin(2\theta) sin(2\omega_L t)}{4 + A_2B_2 + 3A_2B_2 cos(2\theta) cos(2\omega_L t)}. \quad (4)$$

Using such $R(t)$ functions we eliminate some detector-related effects which can cause systematic errors.

If the specific symmetries of the set-up are considered, we arrive to an expression for the $R(t)$ function identical with Eqn. 3. This means that the following combinations between the detectors at $\pm 45^\circ$ and $\pm 135^\circ$ are possible (see Figure 1 for the detector labels): $I_1 = (A + L) \uparrow + (D + G) \downarrow$ and $I_2 = (A + L) \downarrow + (D + G) \uparrow$, where $\uparrow$ denotes filed up and $\downarrow$ field down. Similarly another combination of detectors can be done, but the amplitude of the $R(t)$ function will be reduced and the phase will be shifted. For example,

if the detectors at $\pm 75^\circ$ and $\pm 105^\circ$ with respect to the beam direction ($\pm 30^\circ$ with respect to each other) are considered ($I_1 = (B+K) \uparrow + (C+J) \downarrow$ and $I_2 = (B+K) \downarrow + (C+J) \uparrow$), the $R(t)$ function will have almost the same phase as in Eqn. 3, but twice smaller amplitude

$$R(t,B) = \frac{3A_2B_2 sin(2\omega_L t)}{8 + 2A_2B_2 - 3\sqrt{3}A_2B_2 cos(2\omega_L t)}. \quad (5)$$

For the combination of detectors at $\pm 150^\circ$ with respect to each other, $\pm 45^\circ$ and $\pm 105^\circ$ with respect to the beam, the following time spectra can be considered: $I_1 = (A+L) \uparrow + (C+J) \downarrow$ and $I_2 = (K+B) \uparrow + (G+D) \downarrow$. The $R(t)$ function will have a phase shift and twice smaller amplitude

$$R(t,B) = \frac{3A_2B_2(sin(2\omega_L t) + \sqrt{3}cos(2\omega_L t))}{16 + 4A_2B_2 + 3A_2B_2(3sin(2\omega_L t) - \sqrt{3}cos(2\omega_L t)}. \quad (6)$$

The phase shift of the $R(t)$ function depends on the value of the $g$ factor, while the reduction of the amplitude is fixed for each combination of detectors. This allows a simultaneous fit of all detector combinations using two fit parameters, the Larmour frequency and the amplitude of the $R(t)$ function, which is related to the orientation of the nuclear spin ensemble.

Most of the crystals of the Cluster detectors do not lie exactly in the horizontal plane, but are misaligned at a small angle $\phi$. This causes an additional reduction of the amplitude. However, due to the large distance between the implantation spot and the detector faces, this effect, as well as the influence of geometric factors due to the finite dimensions of the implantation spot, can be neglected. A more elaborate analysis needs to take into consideration the implantation position of each ion, and the crystal of the first hit in a Cluster detector. Here we report results obtained only with detectors at $90^\circ$ with respect to each other, at $\pm 45^\circ$ and $\pm 135^\circ$ with respect to beam axis.

### 3.2 Momentum Selection

In fragmentation reactions the fragments have a longitudinal momentum distribution $exp(-p^2/2\sigma^2)$, with $\sigma = \sigma_0^2 A_{fr}(A_p - A_{fr})/(A_p - 1)$, where $A_p$ and $A_{fr}$ are the mass numbers of the projectile and the fragment, and $\sigma_0 \approx 90 MeV/c$ [9].

The alignment of the nuclear spin ensemble depends on the longitudinal momentum distribution [7]. Under alignment of the nuclear ensemble the different $m$ substates for a given spin $I$, $m = -I, -I+1, ..., I$ have different population, but the $\pm m$ substates are equally populated. Positive (oblate) alignment occurs when the spin ensemble is oriented in a plane perpendicular to the beam axis, while for negative (prolate) alignment the spins are oriented perpendicularly to this plane. It is obvious that a change of the sign of the alignment will result

in a change of the sign of the $R(t)$ function. Experiments at intermediate energies demonstrated that the alignment changes its magnitude and sign from the center towards the outermost wing of the momentum distribution. This effect was studied also theoretically and qualitative understanding was achieved [10]. Therefore, it is necessary to determine the position of the center and wing to eliminate interference effects resulting from mixing of alignment. So far some measurements were done at intermediate energies and such data did not exist at relativistic energies.

The measured momentum distribution with *Sc21* is shown in the left-hand-side of Figure 4. The lower wing was cut with the $S2$ slits of the FRS (see Figure 1). During the experiment the shape of the momentum distribution gradually changed to more complicate form. The reason is that beam which hit scintillator *Sc21* was close to the maximal ($2 \cdot 10^5$ ions/s) and the properties of the scintillator deteriorated. For this reason we deduced the isomeric ratio for the $19/2^+$ isomer in $^{127}$Sn as a function of the momentum distribution and used it as a criterium to define the position of the center and the outermost wing (see Figure 4, right). The isomeric ratio is expected to have a minimum in the center and maximum in the wing of momentum distribution [11].

The isomeric ratio is defined as the probability that in a reaction an isomeric state is excited

$$IR = \frac{Y}{N_{imp}FG} = \frac{N_\gamma(1+\alpha_{tot})}{\epsilon_{eff} b_\gamma N_{imp} FG}, \tag{7}$$

where $N_\gamma$ is the number of counts in the $\gamma$ ray line depopulating the isomer, $\alpha_{tot}$ is the total conversion coefficient for this transition, $b_\gamma$ is its absolute branching ratio, $\epsilon_{eff}$ is the efficiency correction and $N_{imp}$ is the number of implanted ions of the isotope of interest. $F$ and $G$ are the correction factors for the inflight isomer decay and the finite detection time of the $\gamma$ ray, respectively. The isomeric ratio plotted on Figure 4 is the average for the most intensive transitions

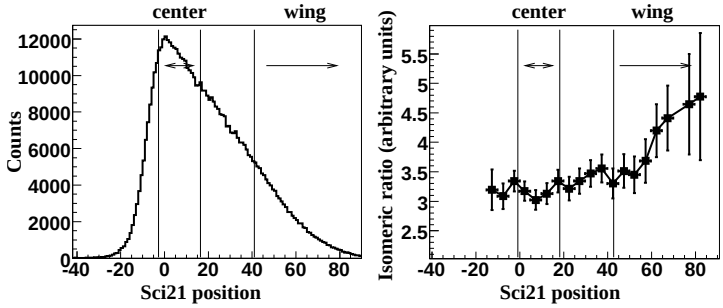


Figure 4. Left: Longitudinal momentum distribution for $^{127}$Sn measured with *Sci21*; Right: The isomeric ratio for the $19/2^+$ isomer in $^{127}$Sn as a function of momentum distribution. The positions of center and wing are indicated with vertical lines.

in $^{127}$Sn, without corrections which do not depend on momentum distribution. At this stage of the analysis it is enough to determine the relative, not the absolute values for the isomeric ratio.

## 4 Results and Discussion

The $R(t)$ functions of the 1095 keV and 715 keV $\gamma$ rays and for different cuts of the longitudinal momentum distribution are presented in Figure 5. The amplitude of the $R(t)$ function, which is sorted for the sum of the time spectra of the 1095 keV E2 and 732 keV M2 transition for the center of the momentum distribution (see the middle section of Figure 5), is very small and has an opposite phase compared to compared to the $R(t)$ function for the outermost wing (see the upper section of Figure 5). This indicates a sign change of the alignment of the nuclear spin ensemble between the center and the wing of the momentum distribution.

The $R(t)$ function for the 715 keV transition was sorted for the outmost wing of the momentum distribution (see the lower section of Figure 5). It display op-

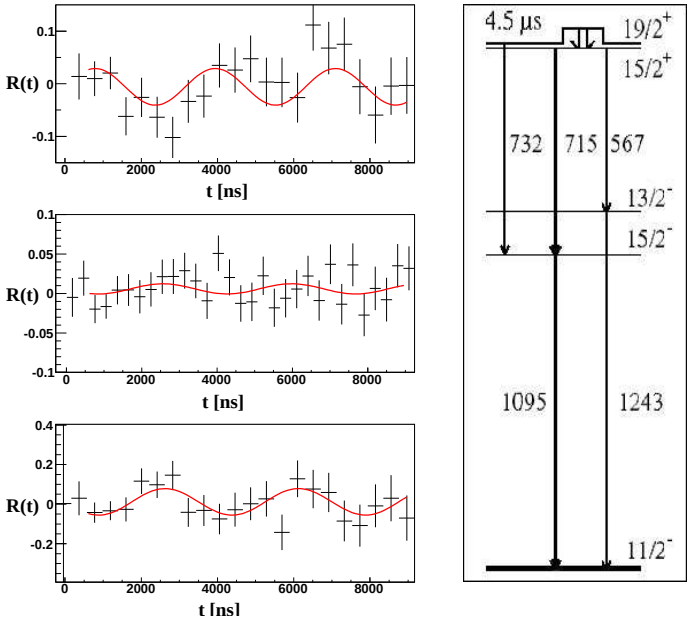


Figure 5. Left: (up) $R(t)$ function for the 1095 keV and 732 keV transitions at the wing of the momentum distribution; (middle) $R(t)$ function for 1095 keV and 732 keV transitions at the center of the momentum distribution; (down) $R(t)$ function for 715 keV transition at the wing of the momentum distribution. Right: Partial level scheme of $^{127}$Sn, revealing the decay of the $19/2^+$ isomer [2].

posite phase, compared to the $R(t)$ function for the 1095 keV transition, which is not in agreement with the published level scheme [2]. According to the published spin and parities, the 715 keV transition should have E1 multipolarity. In such a case its orientation coefficient would be $A_2 = -0.4$, which is similar to the values of the orientation coefficients for the 1095 keV E2 transition, $A_2 = -0.39$, and the 732 keV M2 transition, $A_2 = -0.37$.

Fits of the $R(t)$ functions are displayed in Figure 5. The obtained values of the $g$ factor, $g \approx 0.16$ are in agreement with the theoretical expectations based on the empirical $g$ factors and on large-scale shell model calculations. These results will be discussed elsewhere [12].

For the $R(t)$ function of the 715 keV transition $10^4$ photopeak events were used in the data analysis, which provides the limit for such experiments.

## 5 Conclusions

First results from the g-RISING campaign for the $g$ factor of the $19/2^+$ isomer in $^{127}$Sn from relativistic fragmentation demonstrate that significant alignment ($\sim$10%) is observed in the outermost wing of the momentum distribution. The results indicate that a sign change of the alignment takes place between the center and the wing. The present experiment provides a possibility to set a limit on the feasibility of such measurements in terms of detected $\gamma$-rays, or in terms of the required intensity of the secondary beam, which needs to be $\sim 5 \cdot 10^2$ ions/s for a five-days experiment in case a single $\gamma$ transition would be analysed.

## Acknowledgments

This work was supported in part by the EC EURONS RII3-CT-2004-506065 project and the Bulgarian National Science Fund grant VUF06/05.

## References

[1] H.J. Wollersheim et al (2005) *Nucl. Instr. Meth. Phys. Res. A* **537** 637; www-aix.gsi.de/ wolle/EB_at_GSI/FRS-WORKING/main.html
[2] J.A. Pinston et al. (2000) *Phys. Rev. C* **61** 024312.
[3] J.A. Pinston and J. Genevey (2004) *J. Phys. G* **30** R57.
[4] P. Raghavan (1989) *Atomic Data and Nuclear Data Tables* **42** 189.
[5] W.D. Schmidt-Ott et al. (1994) *Z. Phys. A* **350** 215.
[6] G. Georgiev et al. (2002) *J. Phys. G* **28** 2993-3006.
[7] I. Matea et al. (2004) *Phys. Rev. Lett.* **93** 142503.
[8] H.Geisel et al. (1992) *Nucl. Instr. Meth. B* **70** 286.
[9] A.S. Goldhaber (1974) *Phys Lett* **53B** 306.
[10] N. Coulier et al. (2001) *Phys. Rev. C* **63** 054605.
[11] J.M. Daugas et al. (2001) *Phys. Rev. C* **63** 064609.
[12] L. Atanasova et al. (2006) in preparation.